Ocean Modelling 196 (2025) 102536

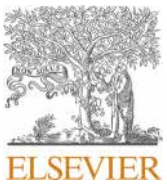

Contents lists available at ScienceDirect

Ocean Modelling

journal homepage: www.elsevier.com/locate/ocemod

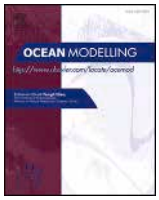

Assessment of the hydrodynamical signature of the record-breaking 2021 flood along the Amazon estuary

Paul Coulet [a,b,*], Fabien Durand [a,b], Alice Fassoni-Andrade [b], Jamal Khan [a], Laurent Testut [c], Florence Toublanc [a], Leandro Guedes Santos [d], Daniel Medeiros Moreira [e,f]

[a] LEGOS, Université de Toulouse, IRD, CNRS, CNES, UT3, Toulouse, France
[b] University of Brasília (UnB), Institute of Geosciences, Brasília, Brazil
[c] LIENSs UMR 7266, CNRS- La Rochelle University, La Rochelle 17000, France
[d] CPRM, Serviço Geológico do Brasil, Avenida Doutor Freitas, Marco, Belém 3645, Brazil
[e] CPRM, Serviço Geológico do Brasil, Avenida Pasteur, Urca, Rio de Janeiro 404, Brazil
[f] GET, CNRS/CNES/IRD/UT3, Toulouse 31400, France

ARTICLE INFO

Keywords:
Amazon
Flood
Estuary
Extreme

ABSTRACT

Since the late 1990s, the hydrological cycle linking the Andes, the Amazon and the Atlantic Ocean has been intensifying. The Amazon estuary is the eastern terminal connection of this hydrosystem, linking the Amazon watershed to the open ocean. At Óbidos, the upstream limit of the estuary, the 2021 May-June flood was recorded as the highest flood in 12 years, with a peak discharge of 260,000 $m^3.s^{-1}$. The impact of this record flood has not been yet quantified along the estuary. This study aims to quantify its signature on estuarine hydrodynamics, using a cross-scale hydrodynamic model of the Amazonian estuarine continuum based on SCHISM. It turns out that the 2021 discharge anomaly (10 % above the seasonal climatology) has a prominent influence on the Amazon River from 800 km to 380 km inland, inducing water level maxima typically 0.3 m higher than during a normal flood year, and about 1 m higher than during a weak flood year. Analysis of the various hydrodynamic factors conducive to the water level maxima along the estuary (i.e. discharge, oceanic tide and atmospheric forcing) shows that this is largely due to the discharge contributing twice as much in 2021 as in a normal year. In contrast, from 380 km inland to the oceanic mouth, both in the north-western arm (the North Channel) and in the south-eastern arm (the Pará) of the estuary, the 2021 flood has no significant impact on the water level maxima dynamics, as the variability is dominated by the oceanic tide.

1. Introduction

Situated in the Amazon lowlands, the Amazon estuary connects the vast upstream watershed to the Atlantic Ocean. It conveys the world's largest freshwater discharge (around 20 %, 200,000 $m^3.s^{-1}$ on average) to the Atlantic Ocean (Callède et al., 2010). The estuary is part of the Andes-Amazon-Atlantic (henceforth AAA) water pathway (Beveridge et al., 2024). This pathway is a complex hydroclimate system with seasonal and interannual variability of its water cycle. Moisture evaporates from the Atlantic Ocean off the Amazon estuary mouth; the evaporation flux being modulated by the climatic variability of the Tropical Atlantic Ocean. Moisture is then transported along "aerial rivers" from the Atlantic Ocean towards the Andes. Along the path of aerial rivers, precipitation is released with particularly high quantities over the Andes mountains. The water then drained from the Andes is the main contributor to the Amazon River mainstem (>90 % contribution), that flows along the Amazon estuary (Beveridge et al., 2024 and references therein).

The Amazon River discharge shows significant seasonal and interannual variability at Óbidos (Fig. 1) due to rainfall variability over the Amazon basin. Seasonal variability is mainly explained by the variability of the location of the Intertropical Convergence Zone (ITCZ) that induces variability in the rainfall integrated over the Amazon Basin (Marengo and Espinoza, 2016 and references therein). In recent years, the Amazon River has been facing a significant change in its hydrological regime, with an intensification of the extreme flood occurrences (Marengo and Espinoza, 2016; Chevuturi et al., 2023). Espinoza et al. (2022) showed that a record flood occurred in 2021 compared to the

* Corresponding author at: LEGOS, Université Toulouse, IRD, CNRS, CNES, UPS, Toulouse, France.
E-mail address: paul.coulet@univ-tlse3.fr (P. Coulet).

https://doi.org/10.1016/j.ocemod.2025.102536
Received 1 October 2024; Received in revised form 7 March 2025; Accepted 11 March 2025
Available online 12 March 2025

recent extreme floods. This flood was due to rainfall exceedance related to intensified circulation of the Walker and Hadley cells over the northern Amazonia situated between 5 °S and 5 °N. This event coincided with a La Niña event in the central Pacific and a positive Sea Surface Temperature in the tropical Atlantic Ocean.

The Amazon estuary stretches from the open ocean to 800 km upstream around Óbidos (Kosuth et al., 2009), where the tidal signal is very reduced. On the 16th of June 2021, 600 km upstream of Óbidos, the water level measured at the Manaus hydrological station was the highest ever during the 1903–2021 period (Espinoza et al., 2022). At Óbidos hydrological station, the river discharge reached 260,000 $m^3.s^{-1}$ the 30th of May 2021 (www.snirh.gov.br/hidrotelemetria/Estacoes.aspx, last access September 2024). For now, we term as the 2021 flood, the 2-month-long discharge peak (Fig. 1) entering at Óbidos centered on the 30th of May. At this time of the year, the whole estuarine region was locked down due to the COVID-19 outbreak. Thus, no in situ gauging station was operating anywhere along the estuary. Consequently, the impacts of the 2021 flood on the Amazon-Pará estuary hydrodynamics remains poorly studied, to date.

Numerically modeling the Amazon estuary dynamics has been a major challenge during the past 20 years. The main complicating factors are its size (>800 km in length), its braided geometry in the terminal delta and the poor knowledge of its bathymetry (Fassoni-Andrade et al., 2023a). Modeling estuarine systems requires tackling a broad spatio-temporal spectrum for their hydrodynamics to be correctly reproduced, with scales typically covering three orders of magnitude in space (from hundreds of kilometers on the oceanic side to hundreds of meters in the narrow creeks and channels of the delta), as well as in time (from intra-daily variability of the tide to pluri-annual variability of the hydrological forcing). This poses strong numerical constraints to modelers. The pioneering works of Gabioux et al. (2005) and Gallo and Vinzon (2005) proposed a numerical model covering the whole Amazon estuarine continuum, based on a rectangular grid with a node spacing ranging from 15 km at the shelf break to 1 km in the estuary. Le Bars et al. (2010) developed an unstructured grid model, with a node spacing ranging from 20 km to 2 km. The model domain covered the downstream part of the Amazon estuary as well as its connection with the Pará River. More recently, Fassoni-Andrade et al. (2023a) developed a high-resolution SCHISM-based model of the Amazon estuary, with a resolution up to 250 m in the Amazon mainstem, comprising the adjoining floodplains and based on an unprecedented bathymetric atlas (Fassoni-Andrade et al., 2021). The model used in this study to assess the hydrodynamical signature of the 2021 flood over the estuary builds on the SCHISM configuration of Fassoni-Andrade et al. (2023a).

Due to the observational gap mentioned above, to the best of our knowledge the following fundamental questions remain unaddressed, to date: how far did this 2021 extreme flood extend towards the downstream part of the estuary? How long did its imprint last? How different was it from a flood occurring during a normal year? To tackle this, we used a hydrodynamical model of the estuary to study the 2021 flood influence on estuarine hydrodynamics, encompassing the whole region from Óbidos to the open ocean. We start by presenting the model configuration and the observational data in Section 2. Then we assess the model ability to represent the main hydrodynamical estuarine processes in Section 3. Section 4 presents the influence of the 2021 flood on water level dynamics along the estuary. Section 5 provides a discussion and conclusion.

2. Data and methods

2.1. 2DH hydrodynamic model of the Amazon estuary

This section focuses on the SCHISM (Zhang et al., 2016) cross-scale hydrodynamic model of the Amazon estuary. The present study uses the modeling framework previously developed by Coulet et al. (2025). The modeling domain encompasses the entire hydraulic continuum from

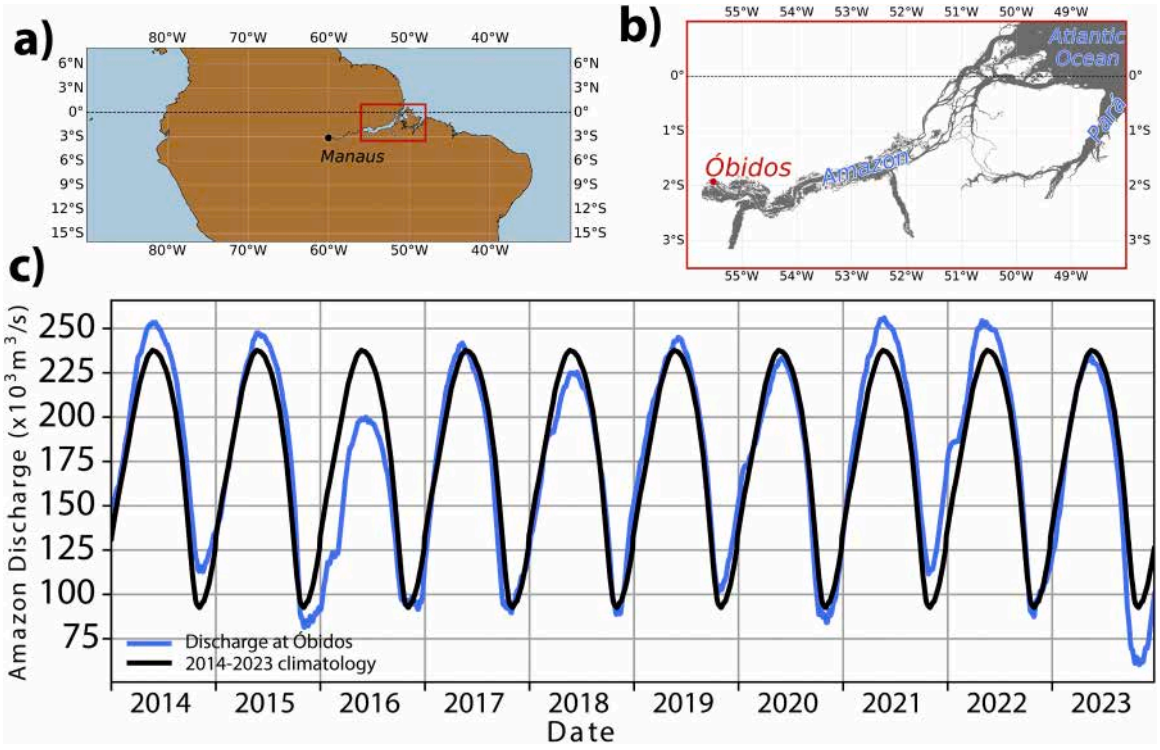

Fig. 1. (a) Location of the Amazon estuary on the Northern Coast of Brazil. (b) The inset map shows the Amazon estuary, the location of the main water bodies and of the gauging station Óbidos. (c) Amazon Discharge derived from water level timeseries observed at Óbidos, the upper limit of the Amazon-Pará estuary (blue line). The black line represents the seasonal climatology of the discharge over the past decade (2014–2023). Data provided by ANA (Agência Nacional de Águas, Brazilian water agency, www.snirh.gov.br/hidrotelemetria/Estacoes.aspx; last access August 2024).

the upstream limit of the estuary, in Óbidos, to the deep Atlantic Ocean. It covers the Amazon River and its adjoining floodplains as well as the Pará River, as is depicted by Fig. 2. We use SCHISM v5.11 (Zhang et al., 2016) in depth-integrated mode.

The domain was discretized on an unstructured triangular mesh with 1,039,864 nodes and 2,024,317 elements. The seamless unstructured grid covers the whole estuary-to-ocean hydraulic continuum (Fig. 2), with an Equivalent Resolution (hereafter ER) encompassing three orders of magnitude, from about 10 m in the inner estuary to >3.6 km offshore (Fig. 3b). The ER of the unstructured grid was computed as $ER = \sqrt{A_t}$, where A_t is the area of the triangle t (Huang et al., 2021). This broad range of ER is designed to enable an accurate characterization of the hydrodynamical processes in areas of interest and to avoid unnecessary mesh refinement to save computational time. The size of the elements is defined locally from a criterion based on the local bathymetry and its gradient, following Krien et al. (2016), to capture properly the dynamics of the high frequency gravity waves such as the tide. The model geometry relies on the recent topographic-bathymetric atlas from Fassoni-Andrade et al. (2021). This high-resolution (30 m) composite atlas has been shown to accurately describe the bathymetry of temporarily-flooded areas of the Amazon estuary, with in particular a RMSE of 1.2 m over the downstream floodplains.

The model is forced at its open boundaries by the XTRACK altimetric tidal constituents (Birol et al. 2017; available at www.aviso.altimetry.fr/en/data/products/auxiliary-products/coastal-tide-xtrack.html, last access October 2023) in the open ocean. Consequently, the open ocean boundaries are aligned with Topex/Jason altimetric tracks. This approach has been adopted in the hydrodynamical modeling of similar tropical deltas (Testut and Unnikrishnan, 2016). The tidal constituents imposed are M2, N2, K2, S2, 2N2, O1, K1, Q1, P1, MF, Mm, M4, MS4, M6, NU2, MU2, T2, SA, SSA, MN4, S1, S4, M3, R2, MSf and J1. We also considered the astronomical tidal forcing over the modeling domain with the tidal potential of K1, K2, L2, M2, MU2, 2N2, N2, NU2, O1, P1, Q1, S2 and T2. The tidal constituents considered to force our model capture 99 % of the total tidal variability observed at Escola do Igarapé Grande (station 7 in Fig. 2) near the Amazon mouth (not shown). We forced the model by the observed discharge for the open boundaries in fluvial regions (Amazon, Xingu and Tapajós in the Amazon region, Tocantins, Capim and Guamá in the Pará region) (Fig. 3b). For the tributaries where no discharge data was available (at locations (50.98°W, 2.07°S), (50.83°W, 2.01°S) and (48.48°W, 1.58°S)), a Flather (1976) radiation boundary condition has been applied. The atmospheric forcing is prescribed over the model domain with atmospheric pressure and wind from a 6-hourly CFSR reanalysis at 0.5° resolution (Saha et al.,

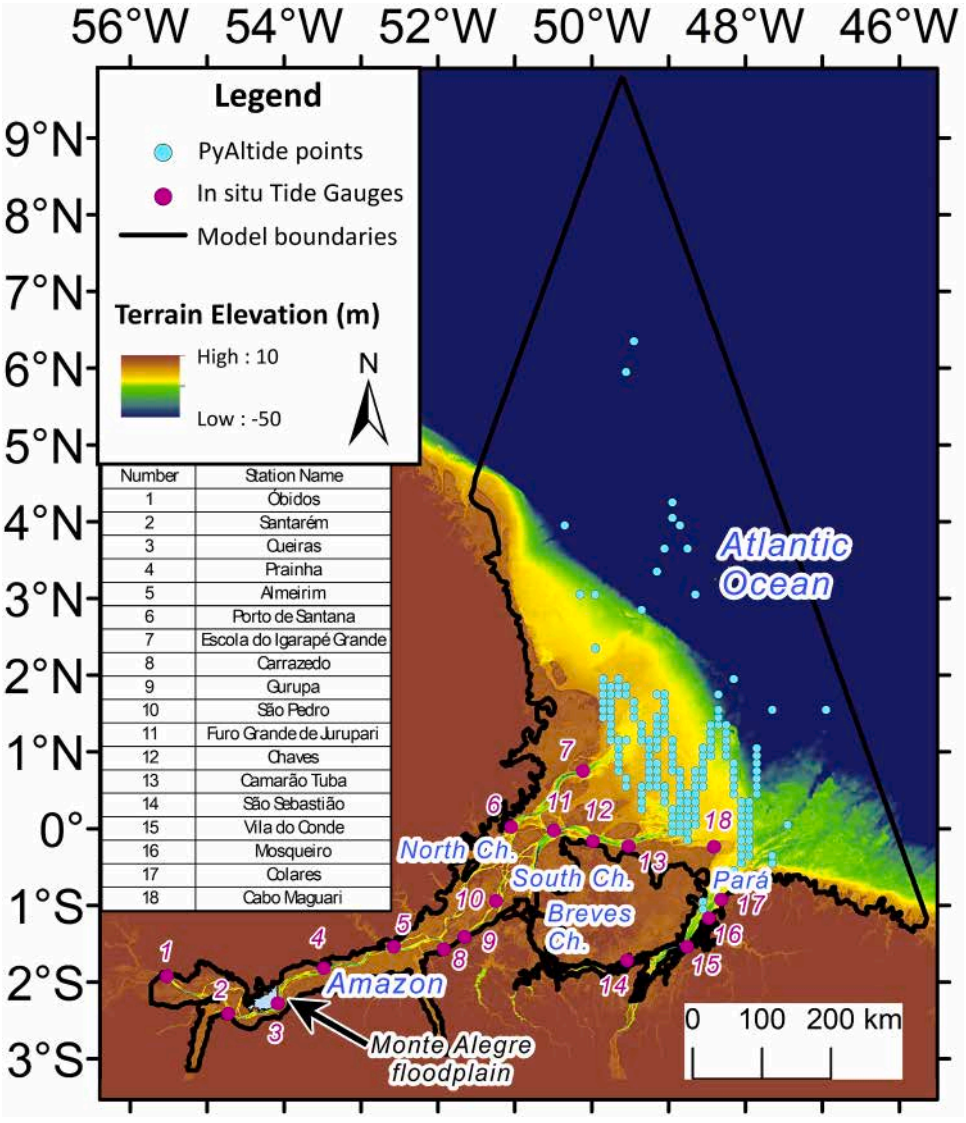

Fig. 2. Bathymetry of the Amazon estuary. Bullets mark the location of the tide gauges used to assess the model performance. The purple ones show the in situ tide gauge stations. The blue ones show the oceanic virtual tide gauge stations from the PyAltide product.

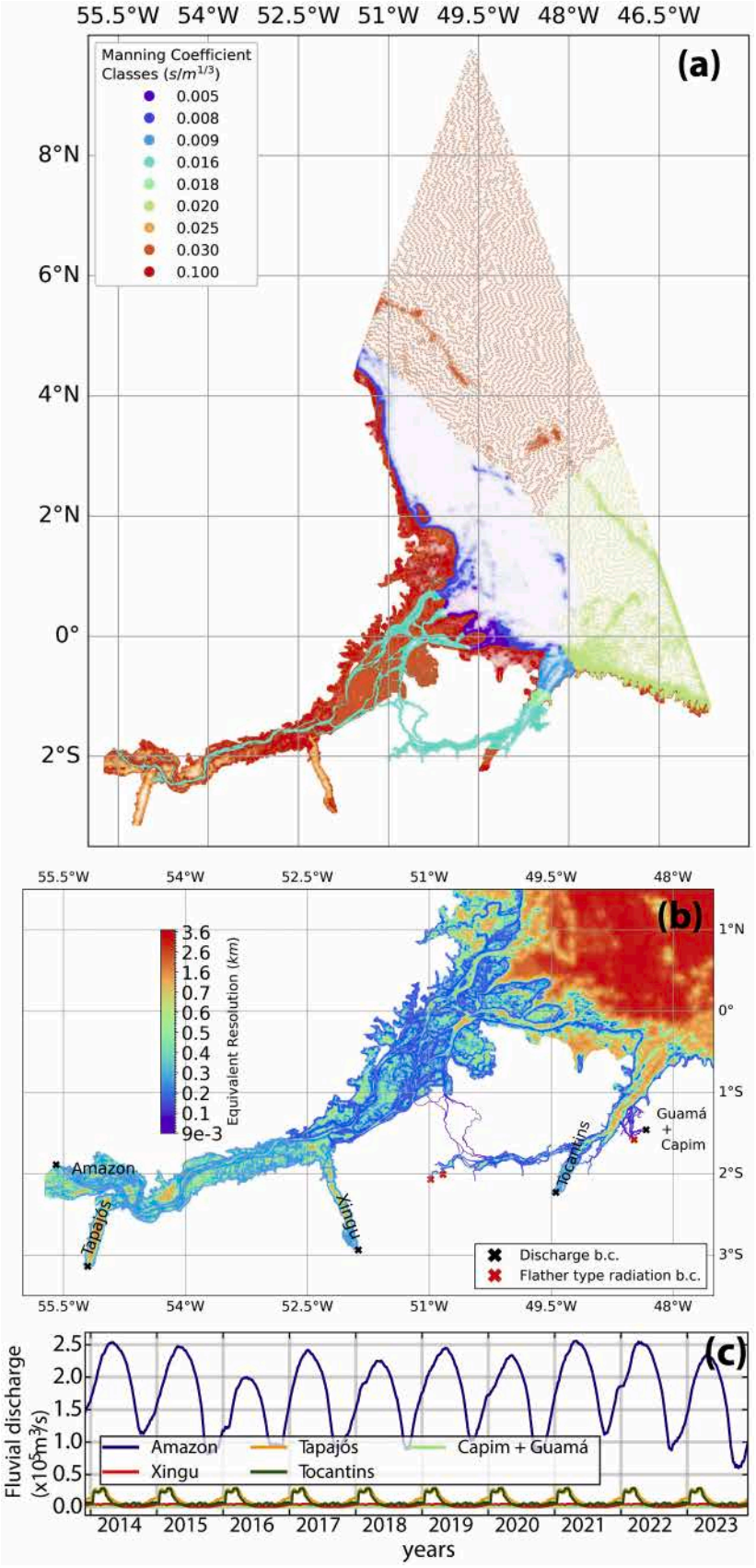

Fig. 3. (a) Distribution of the Manning's bottom friction coefficient over the model domain. (b) Equivalent resolution of the unstructured model grid. Black crosses locate the open boundaries with river discharge boundary condition (b.c.) and the respective river names. Red crosses locate open boundaries with Flather type radiation boundary condition. (c) Discharge time series for the different tributary rivers of the model over the period 2014–2023.

2011). After sensitivity tests, the timestep of the model was set to 400s.

To study the water level dynamics over the past decade and keeping in mind our specific interest in the 2021 flood, we simulated the period 01/11/2013 to 01/01/2024. We discarded the first two months to allow for the spin up of the model. A reference simulation (*REF*) was conducted with all the water level forcing factors considered in our model (river discharge, tide, atmospheric pressure and surface wind). We also conducted a sensitivity experiment without atmospheric forcing (*NOATM*), deactivating the effects of the atmospheric pressure and surface wind. We ran the model year by year, hot-starting it from the end of the previous year simulation to account for the effect of the 18.6-year nodal cycle on the modulation of the tidal potential (Pugh and Woodworth, 2014).

2.2. In situ tide gauges data

For calibration and validation of our model, we considered a comprehensive dataset of in situ and spaceborne water level records. Tide gauges records scattered all along the estuarine continuum (Fig. 2), consisting both of historical and recent observations, were used for validation of the tidal characteristics and the Mean Water Level (MWL). This dataset consists of high-frequency (typically 10 min) bottom pressure sensor records across the whole Amazon-Pará estuary and allows for the analysis of the main tidal constituents propagating along the Amazon estuary. Some of these records are referenced to EGM08 geoid model (Callède et al., 2013) and were used to assess the model's ability to reproduce the MWL spatial variability across the Amazon River.

2.3. Altimetric virtual tide gauges

Altimetric virtual tide gauge stations located off the mouths of the delta, spanning the whole continental shelf and slope, were also considered for the validation of the tide (blue bullets in Fig. 2). They come from a recently developed altimetric tidal atlas called PyAltide. This regional tidal atlas covers the Amazon and Pará mouths and the continental shelf offshore the mouths (corresponding to the coastal part of our modeling domain). To develop this dataset, Sea Level Anomalies (SLAs) were extracted from multi-mission Along-Track Sea Level Anomalies regional products (X-TRACK-L2P, Birol et al. (2017); available at https://www.aviso.altimetry.fr/en/data/products/sea-surface-height-products/regional/x-track-sla/x-track-l2p-sla-version-2022.html; last access May 2022) with a data coverage of nearly 30 years (1993–2020). Tidal constituents were then computed using UTide (Codiga, 2011). This dataset enables a comprehensive observability of the coastal tide, in a region where historical tide gauges records are extremely scanty (Gallo and Vinzon, 2005; Le Bars et al., 2010; Coulet et al., 2025).

This combined in situ and remotely sensed water level dataset constitutes the most comprehensive tidal dataset of the Amazon-Pará estuarine continuum, with unprecedented coverage from the upstream estuary to the oceanic region.

2.4. Bottom friction parameterization

Momentum dissipation by bottom friction in our SCHISM configuration is parametrized through a Manning formulation. The spatial distribution of Manning coefficient over the modeling domain is shown on Fig. 3a. Particular attention has been given to adjust this parameter, as it plays a crucial role in the accuracy of the numerical modeling of the Amazon estuary (Le Bars et al., 2010). Starting from Fassoni-Andrade et al. (2023a) mapping of the Manning coefficient, we conducted 20 sensitivity experiments to further calibrate the Manning coefficient values. Each experiment consisted of a 1-year long simulation of the year 2020 (a rather normal year for the last decade in terms of Amazon River discharge, as seen from Fig. 1). We focused on the assessment of the accuracy of the model with regards to the tidal propagation, characterized by the amplitude and phase of the dominant constituents at the tide gauges stations. The representation of the MWL was also assessed where vertically referenced tide gauges stations were available.

Inside the estuary, the tidal characteristics must be validated considering the seasonal variability of the river discharge, as it interacts with the tidal waves and modulate their amplitude and phase (Kosuth et al., 2009; Fassoni-Andrade et al., 2023a). To this end, we focused on the amplitude and phase of the two main astronomical tidal constituents of the estuary, namely M2 and S2 (Gallo and Vinzon, 2005), over two 32-day period, during flood season (01/05/2020 to 02/06/2020) and drought season (01/11/2020 to 03/12/2020). This time span allows the separation of the main tidal constituents in the harmonic analysis (Pugh and Woodworth, 2014). For the oceanic part, such a seasonal modulation of the tide is not significant (Gallo and Vinzon, 2005; Durand et al., 2022), therefore we performed a one-year harmonic analysis over the year 2020 of the modeled tidal constituents.

For validation, the amplitude difference and phase difference were computed for the dominant tidal constituents. Then, the tidal simulation accuracy at the estuarine stations was assessed by calculating the Complex Error (CE) (Andersen et al., 1995), defined as below:

$$CE = \frac{1}{\sqrt{2}} \left| A_m e^{i\theta_m} - A_o e^{i\theta_o} \right| \tag{1}$$

where A denotes the amplitude of the tidal constituent and θ its phase. m stands for modeled and o for observed. In our case, we calculated a total complex error for the two main semi-diurnal constituents M2 and S2. Eq. (1) becomes:

$$CE = \sqrt{\frac{1}{2} \sum_{M2,\ S2} \left| A_m e^{i\theta_m} - A_o e^{i\theta_o} \right|^2} \tag{2}$$

From this, we derive the Percent Error (PE) as follows:

$$PE = \frac{CE}{A_{observed\ M2+S2}} \times 100 \tag{3}$$

Here, $A_{observedM2\,+\,S2}$ is the sum of the observed amplitude of M2 and S2 during flood season or drought season, as it is a proxy of the mean tidal amplitude in semi-diurnal tidal regimes (Pugh and Woodworth, 2014).

The resulting distribution of the Manning coefficient over our modeling domain is shown on Fig 3a. The calibration process to minimize the CE through trial-and-error resulted in a heterogeneous spatial distribution that distinguishes the northern open ocean and the eastern open ocean (the orange and green zones in Fig. 3a). Additionally, the Pará mouth and Amazon mouth both have variable transition zones (dark blue, purple and turquoise zones at the estuary mouth in Fig. 3a). A distinction has also been made between the northern and southern channels of the Amazon delta (purple and dark blue zones at the Amazon River mouth). This distribution is consistent with the known geological patterns in the open ocean, including the extended fluid mud layer located off the mouths of the Amazon and further to the North along the coast (dark blue zone in Fig. 3a) (Kineke and Sternberg, 1992, 1995; Nittrouer et al., 1996).

2.5. Water level dynamics assessment variables

To study the signature of the 2021 flood on estuarine hydrodynamics, we focused mainly on two indicators. On the one hand, we considered the yearly water level maxima reached during 2021, along the mainstems of the estuarine network (namely the North channel of the Amazon, and the Pará river). On the other hand, specifically in the upstream part of the Amazon estuary where wide floodplains are located (Fassoni-Andrade et al., 2021), we assessed the temporal evolution of the volume of water stored in these floodplains. This quantity is tightly linked to the flooding hazard of the riparian communities living on the banks of these intermittently inundated areas. It also has strong

implications on the ecology of the floodplains (Junk et al., 2014). The water volume is calculated within the contour of the floodplain, defined using GEDI (Potapov et al., 2021) water bodies classification.

Yearly maxima are defined as the water levels exceeding the 99.5 percentile of the yearly water level distribution. This corresponds to the 44 h with the highest water levels throughout the year. This approach has already been applied in our previous study about the dynamics of yearly maxima across the Amazon estuary (Coulet et al., 2025) and was commonly used in many past studies of sea level extremes in coastal areas (e.g. Zhang et al., 2000; Haigh et al., 2010; Lyddon et al., 2018b).

To ascertain the imprint of the 2021 flood on the variability of the water level, we quantified the various forcing factors at play in generating extreme events. Our previous study (Coulet et al., 2025) showed that in the Amazon estuary, the discharge, the tide and the atmosphere (essentially the wind) altogether play a significant role in generating water level yearly maxima. Building on this methodology, we isolate the various forcing factors of the water level maxima, as follows. The tide contribution $TIDE_{contribution}$ is the modeled tide during the maxima, computed from a harmonic analysis of *REF* simulation, considering the 8 dominant tidal constituents, which are M2, S2, N2, Mm, MSf, M4, MS4 and MN4. These constituents are computed daily through a 32-day window harmonic analysis of the water level centered on that day using UTide (Codiga, 2011). They explain more than 96 % of the tidal signal throughout every hydrological year along the course of the estuary (not shown). The atmospheric contribution $ATM_{contribution}$ is the water level difference between the *REF* and the *NOATM* simulations:

$$ATM_{contribution} = REF - NOATM \tag{4}$$

Finally, the discharge contribution $DISCH_{contribution}$ is assessed in the following way:

$$DISCH_{contribution} = \left(NOATM - climato_{2014\_2023}(NOATM) - TIDE_{contribution}\right) \tag{5}$$

Where $climato_{2014\_2023}(NOATM)$ is the seasonal climatology of the *NOATM* simulation water level computed over 2014–2023 period after filtering the effect of the tide by applying a 28-day running mean. We term as *ANOMALY* the water level difference between *REF* and $climato_{2014\_2023}(NOATM)$

$$ANOMALY = REF - climato_{2014\_2023}(NOATM) \tag{6}$$

3. Validation of the hydrodynamical model

In a previous study (Coulet et al., 2025), we assessed the model's ability to reproduce yearly water level maxima with regards to in situ observations. Our model appears to accurately capture these extreme events, with a RMSE of 10 cm or less, both in the downstream part of the estuary and in its upstream part. In this study, we firstly focused on the propagation of the tide across this hydraulic continuum, its amplitude and phase being modulated by the geometry of the domain (local bathymetry, coastal shoreline and riverbanks delimitation) (Dronkers, 1964) and the interaction with the river discharge (Dronkers, 1964; Godin, 1985, 1999). We then evaluated the performance of the model on representing the MWL slope along the estuary. Finally, the ability of the model to simulate the seasonal behavior of the intermittently flooded areas was addressed. This was done through the comparison between the observed Water Presence Seasonality (hereafter WPS) and the model counterpart. The WPS is defined as the number of months when water was present in a given pixel during 2021. To do so, the WPS of the Monte Alegre floodplain observed in 2021 was extracted from the optical-based Landsat Global Surface Water Monthly Water History (Pekel et al., 2016; available at https://global-surface-water.appspot.com; last access August 2024) (Fig. 7a). This product has a 30 m horizontal resolution.

Our strategy is in line with recent recommendations about coastal modeling (Zhang et al., 2024) and state-of-the-art estuarine model validation protocols (Matte et al., 2017), which advocate for favoring calibration and validation based on the assessment of hydrodynamical processes for cross-scale hydrodynamic systems.

3.1. Tidal characteristics

3.1.1. Oceanic tide

The modeled semi-diurnal tides M2 and S2 are compared with the altimetry-based tidal atlas from PyAltide (Fig. 4). M2 and S2 amplitude and phase at the comparison points were computed using UTide Harmonic Analysis (Codiga, 2011) both for modeled and observed data. A positive (negative) anomaly means that the model overestimates (underestimates). The amplitude of M2 and S2 simulated by the model in the background of Fig. 4a, b, c and d are calculated using the COMODO Toolbox (Allain, 2016)

The differences in the number of evaluation points of M2 versus S2 are linked to the observability of each constituent by the spaceborne altimetry. It is inherent to the specific sampling of the various altimetric satellites as well as the frequency of the constituents (Fang et al., 2004; Pugh and Woodworth, 2014). Indeed, S2 being with a period of 12h00, it is not observable by any sun-synchronous satellite mission such as ERS, ENVISAT, SARAL (35.0-day repetitivity period) or Sentinel3 (27.0-day repetitivity period) – which effectively reduces the number of points where a reliable estimate could be obtained in PyAltide.

Two zones of coastal amplification of M2 and S2 constituents can be observed, centered around (50.5 °W, 2 °N) and (47 °W, 0.5 °S). This is mainly because the continental shelf is suitable for semi-diurnal resonance (Beardsley et al., 1995). For the northern part (around 50 °W, 2 °N), M2 and S2 amplitudes reach 3.75 m and 1.2 m respectively, while for the southern part (around 47 °W, 0.5 °S) it reaches 1.8 m and 0.6 m respectively. One can also denote another amplification area at the entrance of the Amazon mouth (around 0.5 °N, 49.5 °W), reaching respectively for M2 and S2 an amplitude of 2.3 m and 0.65 m. These macrotidal zones with M2 being the dominant constituent are consistent with the past studies (Beardsley et al., 1995; Le Bars et al., 2010; Ruault et al., 2020).

At the Amazon mouth (between 50 °W and 48.3 °W), the M2 amplitude is mainly overestimated, with biases mostly ranging from 3 cm (+3 %) to 19 cm (+12 %), with two areas of larger overestimation corresponding to the resonating areas of M2 tide at the northern part of the estuary (amplitude up to +22 %) and at the Amazon mouth (+28 %). The S2 amplitude there is also mostly overestimated by 4 cm (+11 %) to 6 cm (+17 %). For the Pará River (between 48.3 °W and 47.7 °W), M2 amplitude is roughly in line with the observed values (between −1 % and +6 %) and tends to be underestimated at the very entrance of the Pará mouth with a minimum up to −9 %. As for S2, the scarce number of observations in this area reveals a differing behavior with areas of overestimation and underestimation ranging between −5 % and +30 %.

Considering the phase in Fig. 4c and d, M2 propagation is mostly lagging by 5 ° (10 min) with values ranging from − 20 ° to 10 °. Off the mouth of the southern channel of the Amazon around (0.2 °N, 48.8 °W) the model is rather in phase lead of around 2 ° (4 min). S2 propagation is mostly lagging by 3 ° (6 min), with maximum up to 40 min.

Far from the coast, the M2 amplitude and phase errors exhibited by our model are lower than those previously published for hydrodynamic models of the estuary (e.g. Le Bars et al., 2010). As for the M2 and S2 amplitudes at the stations nearshore, our model is in keeping with previous studies (Gallo and Vinzon, 2005). Globally, M2 and S2 relative amplitude differences and phase differences are similar, as the response of the shelf region is expected to be the same for those two tidal constituents (Beardsley et al., 1995).

3.1.2. Estuarine tide

The propagation of the tide inside the estuary was assessed in depth as the present study focuses specifically on the dynamics of the flood along the course of the inner estuarine network. Coulet et al. (2025) assessed the observed and modeled amplitudes and phases of all the tide

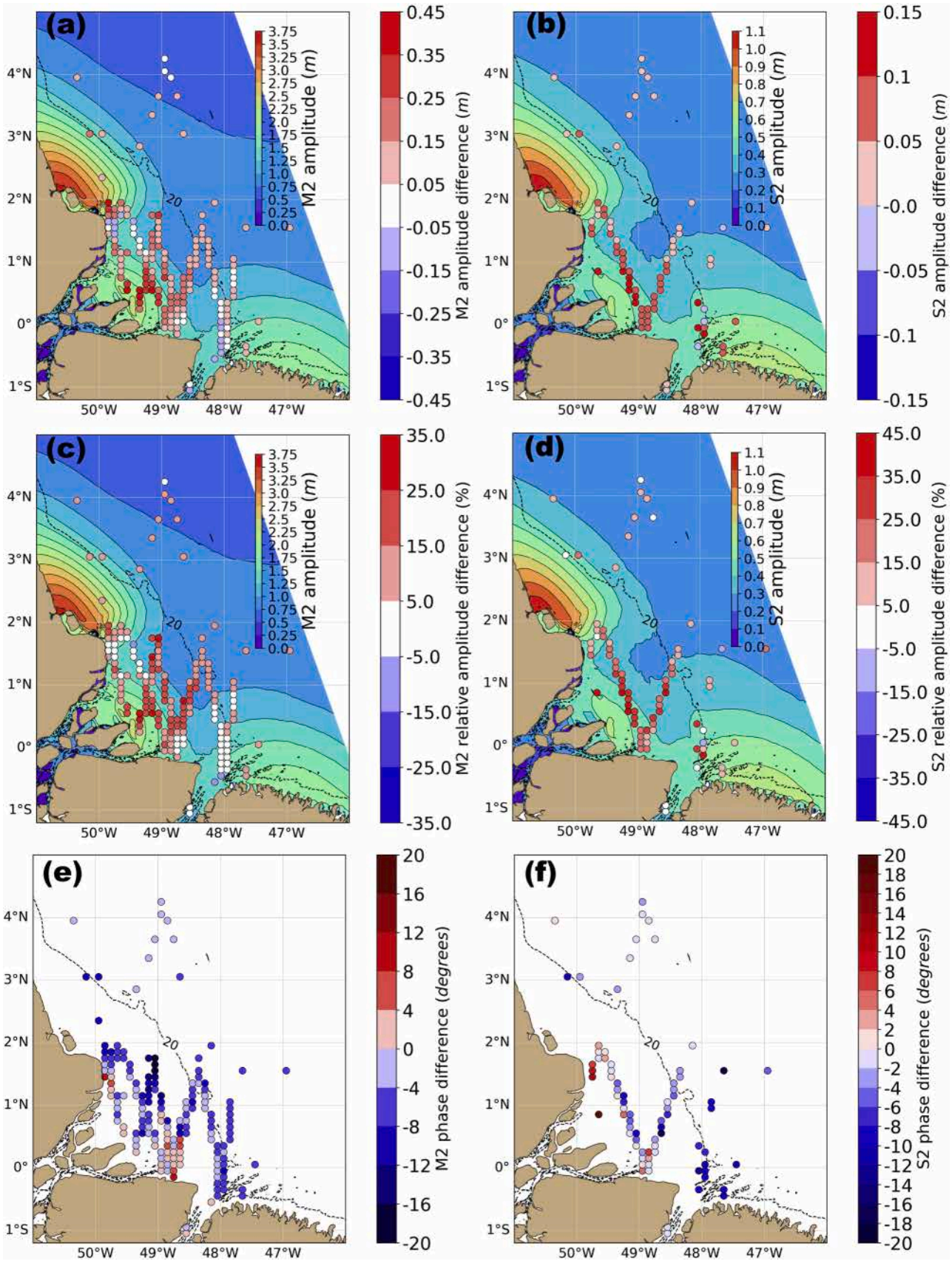

Fig. 4. *amplitudedifference* = $amplitude_m - amplitude_o$ of the main oceanic tidal constituents M2 (a) and S2 (b). *m* refers to the tidal constituents analyzed from the model and *o* refers to the tidal constants extracted from PyAltide tidal atlas. The amplitude of M2 and S2 tidal constituents simulated by the model are displayed in the background of (a) and (b). *relative amplitude difference* = $\frac{amplitude\ difference}{amplitude_o} \times 100$ of M2 (c) and S2 (d) tidal constituents. *phasedifference* = $phase_m - phase_o$ of M2 (e) and S2 (f) tidal constituents.

gauges stations, for five main tidal constituents (M2, S2, Mm, MSf and M4). In this study, we focused on the validation of the semi-diurnal constituents, M2 and S2.

Fig. 5 provides an overview of the tidal properties of the modeled estuarine tide and its validation against in situ data, separately for the drought season and the flood season. The spatial variability of the M2 and S2 total complex error (Eq. (3))) along the estuary is displayed in Fig. 5a and b.

Fig. 5c and d show the complex error at a station compared with the sum of the observed amplitude of M2 and S2 in the Amazon North channel (pink line in Fig. 5b) and in the Pará River (green line in Fig. 5b). The Amazon South Channel is not analyzed as the behavior of the tide is like that of the North Channel (not shown). As shown in Fig. 5b, the model reproduces the tidal modulation along the seasonal cycle in the Amazon North Channel. Indeed, the amplitude of the semi diurnal tides becomes sub-decimetric upstream of 600 km inland in high flow; this limit is shifted to 700 km inland in low flow. This stands in line with past studies about the seasonal variability of the Amazon estuarine tide (Gallo and Vinzon, 2005; Fassoni-Andrade et al., 2023a).

The model replicates the observed M2 and S2 tides with good accuracy over the modeling domain with similar performance in flood and drought season, with a mean complex error of 13.1 cm and 12.9 cm respectively. For the Amazon North Channel, either in flood or in drought season, we can denote that the percent error remains below 20 % until 500 km inland and increases more upstream as the tidal amplitude diminishes.

For the Pará river, the amplitude of the semi-diurnal tides remains mostly the same in flood and drought season. The Pará River does not have an extended watershed of itself. It takes the form of a hydrographic network that receives the flow from several water outlets (Amazon River through Breves Channels, Tocantins, Capim and Guamá for the main tributaries) (Callède et al., 2010; Rosário et al., 2016 and references therein). Its largest tributary, the Tocantins, has a discharge typically inferior to the Amazon by 2 orders of magnitudes (Fig. 3c). Other than that, the model satisfactorily captures the tidal propagation with a complex error under 20 % for both seasons. As for comparison, the model outperforms the latest Amazon-Pará estuary hydrodynamic model (Le Bars et al., 2010) that had a typical bias of 1 m for the M2 amplitude in the Pará River.

The overall improved performance of the model in representing tidal propagation is in accordance with the state-of-the-art modeling of the large tropical estuaries such as the Mekong delta (Eslami et al., 2019) or Bengal delta (Khan et al., 2020). The performance of our model in capturing the tidal characteristics is slightly better than that of Fassoni-Andrade et al. (2023a), which can be attributed to the regional tuning of the Manning's coefficient presented in Fig. 3a.

3.2. Mean water level (MWL)

The simulated and observed MWLs along the North and South Amazon Channel are presented in Fig. 6. The observed values are extracted from Callède et al. (2013). They originate from in situ surveys conducted between 1999 and 2009. They were referenced with respect to EGM08 geoid and should be considered with a possible bias of the order of magnitude of 10 cm due to the composite origin of the datasets used to compute these values (Callède et al., 2013).

The model has a negative bias along the Amazon North Channel with − 0.23 m in Óbidos, − 0.5 m in Porto de Santana and around − 0.3 m for the rest of the stations. The mean water slope fits well the observations as shown in Table 1, with a mean value of about 10 mm.km^{-1} and differences of the order of 0.1–0.7 mm.km^{-1}. For the Southern Channel, the model overestimates the observed MWL at Gurupá station by 0.18 m.

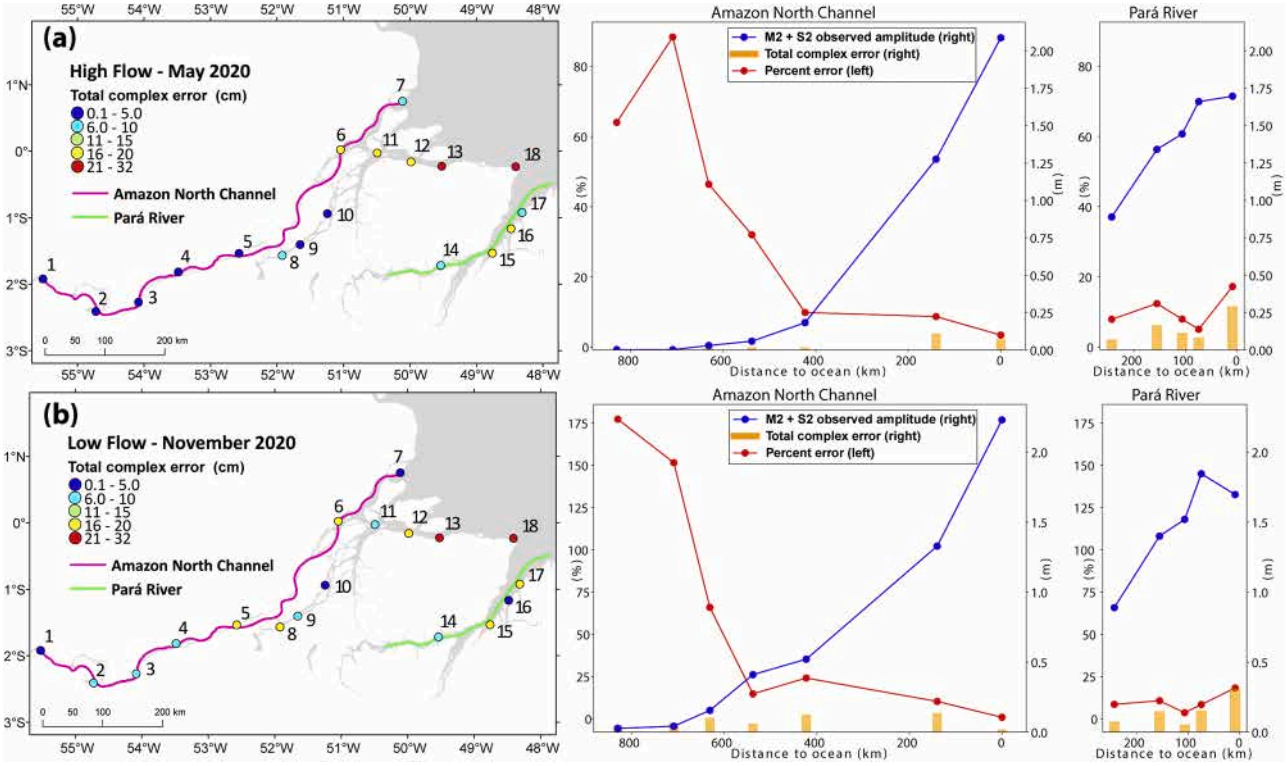

Fig. 5. Total complex error of M2 and S2 along the Amazon-Pará estuary during (a) high flow (May 2020) and (b) low flow (November 2020). Left panels show the spatial distribution of the total complex errors at the tide gauges. Right panels show the sum of the observed amplitude of M2 and S2 at each station, the total complex error and the percent error along the Amazon North channel (pink line) and Pará River (green line).

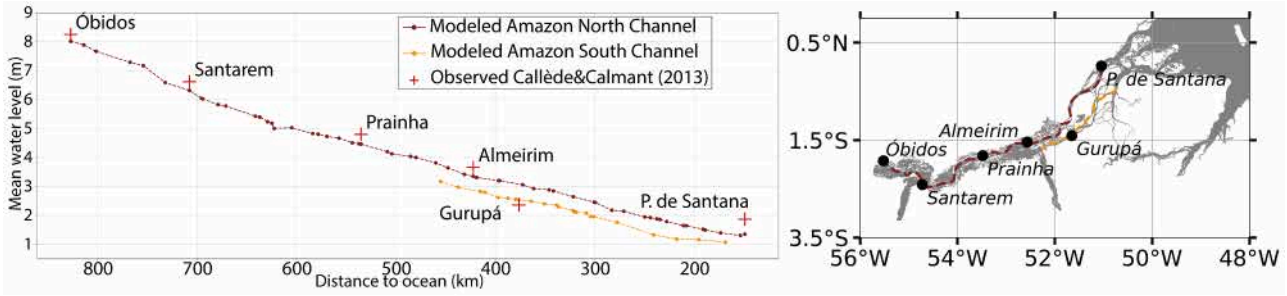

Fig. 6. (left) Observed (red crosses) and modeled (dotted line) MWL along the Amazon River computed as a function of the distance between the gauging station and the Ocean. Observed MWL is extracted from Callède et al. (2013). Modeled MWL is computed as the average water level during the 2014–2023 period. (right) Location of the gauging stations considered along the Amazon estuary.

Table 1
Observed (Callède et al., 2013) and modeled water slopes over the successive reaches in the Amazon Northern Channel.

	Section	Óbidos - Santarem	Santarém - Prainha	Prainha-Almeirim	Almeirim – P. de Santana
Water Slopes (mm. km^{-1})	Observed	14.2	10.7	9.87	7.31
	Modeled	14.1	10.1	9.73	8.04

3.3. Floodplain dynamics: 2021 water presence seasonality of the Monte Alegre floodplain

The Monte Alegre floodplain is situated in the upper estuary around 650 km upstream of the ocean (Fig. 2) along the northern bank of the Amazon, downstream of Santarém. This intermittently inundated area covers about 750 km^2, with a relatively flat bottom (Fig. 7d), with a 4 m elevation over the central part, reaching up to 6–7 m around its periphery. The geometry of the floodplain is complex, with narrow channels originating from the Amazon mainstem irrigating it through the levees that border its southern and eastern flanks. It is observed that the center of the floodplain was consistently flooded (12 months out of 12)

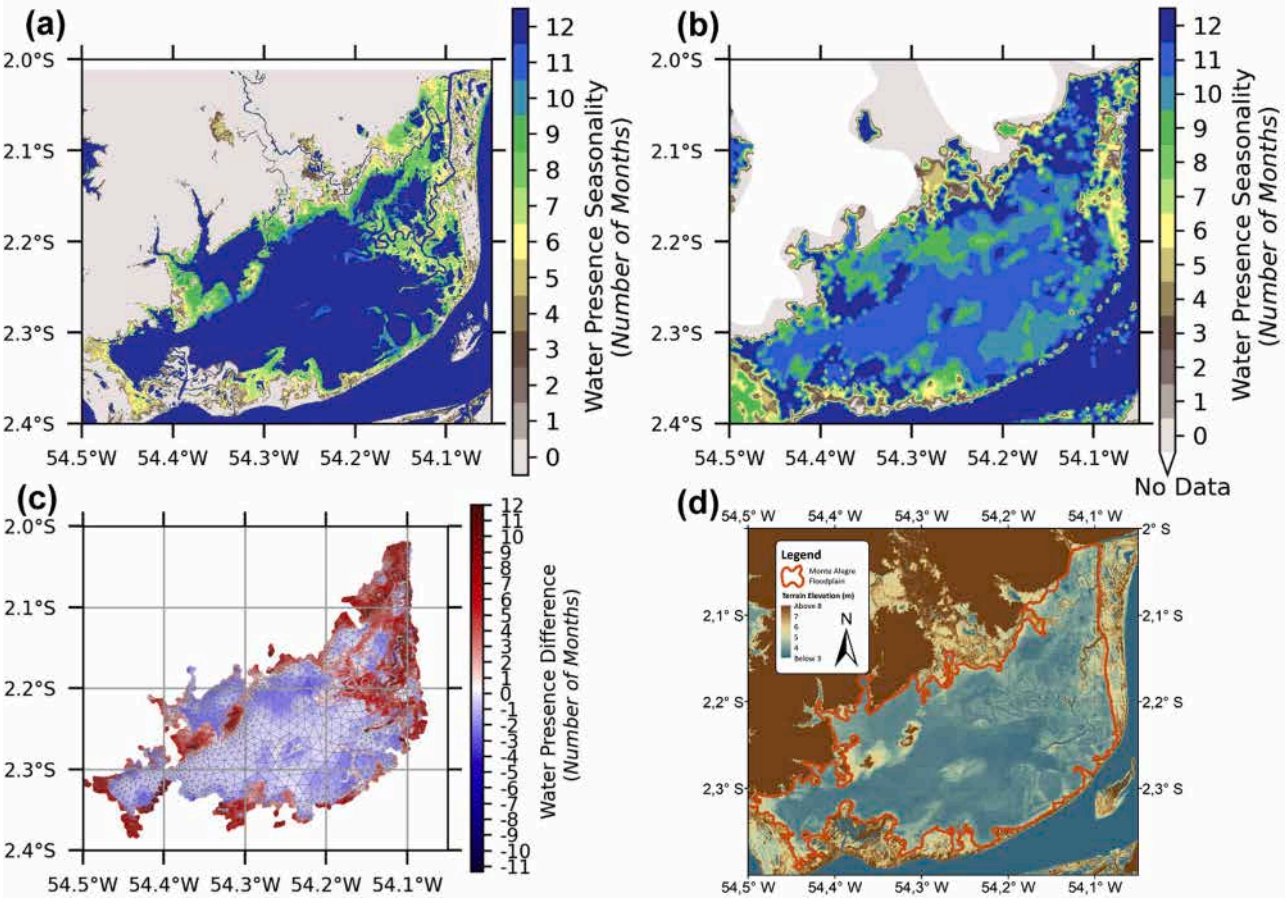

Fig. 7. (a) WPS map of the Monte Alegre floodplain of 2021 from Pekel et al. (2016) derived from Landsat imagery data (0 = always dry; 1 to 12 = inundated from 1 to 12 months of the year 2021). (b) Modeled WPS map for 2021. (c) Water Presence Difference = WPS (Pekel et al., 2016) – Modeled WPS over the Monte Alegre floodplain. The difference is computed at each pixel point of Pekel et al. 2016 product, comparing the observed WPS at the pixel location with water presence of the overlying triangle of the model. (d) Location of the Monte Alegre floodplain with topography bathymetry from Fassoni-Andrade et al. (2021).

in 2021 (Fig. 7a). As we approach the edges of the floodplain, the depth decreases, and the water presence decreases gradually to 8 months (green shades) and 1–2 months (light brown). The levees located between the Amazon and the floodplain, as well as the northwestern rim of the floodplain, remain dry throughout the year.

The 2021 modeled WPS is presented in Fig. 7b. The model captures the inhomogeneous pattern of water presence at the scale of the whole floodplain, with greater water presence (typically around 10 months out of 12) throughout the central part, and values gradually decreasing towards the periphery. Still, a detailed examination reveals marked differences with the observations, at finer scale. The sharp contrasts observed in the north-eastern part of the floodplain, that mirror the topographic gradients, are largely absent in the model. The seasonality of the water presence is mostly underestimated by the model in the central part of the floodplain with roughly 10 % less occurrence (Fig. 7c). This is consistent with the known negative bias of the model MWL in this region. As for the banks of the floodplain, the model rather overestimates the water presence, possibly due to its too coarse resolution that does not allow to capture the fine topographic features as shown in Fig. 7b. One also has to keep in mind that the bathymetry used in our modeling has a typical accuracy of the order of 1.2 m in the floodplains (Fassoni-Andrade et al., 2021). This level of accuracy, although typical of the spaceborne topography over floodable areas (Fassoni-Andrade et al., 2020), also contributes to the overall mismatch between the modeled WPS and the observed one.

Keeping these biases in mind, the capability of the model to capture the large-scale pattern of WPS in the floodplain motivated us to further investigate its behavior in this intermittently-flooded area, considering the specific flood extreme of 2021 presented in the next section.

4. Results: consequences of 2021 flood on the estuarine hydrodynamics

This section focuses on the evaluation of the imprint of the record-breaking flood of 2021 on the hydrodynamics of the estuarine continuum, from its upstream limit in Óbidos down to its oceanic outlet 800 km downstream. The peak discharge observed at Óbidos that occurred on May 30th, 2021 (260,000 $m^3.s^{-1}$), corresponds to the highest observed discharge in 12 years, and second highest in 56 years (www.snirh.gov.br/hidrotelemetria/Estacoes.aspx, last access September 2024). Our approach is twofold: first, we investigated the spatio-temporal pattern of water level maxima simulated by the model during the year 2021 across the estuary. Then we investigated more in depth the hydrodynamics at play during this extreme flood, looking at the water level and floodplain water volume dynamics.

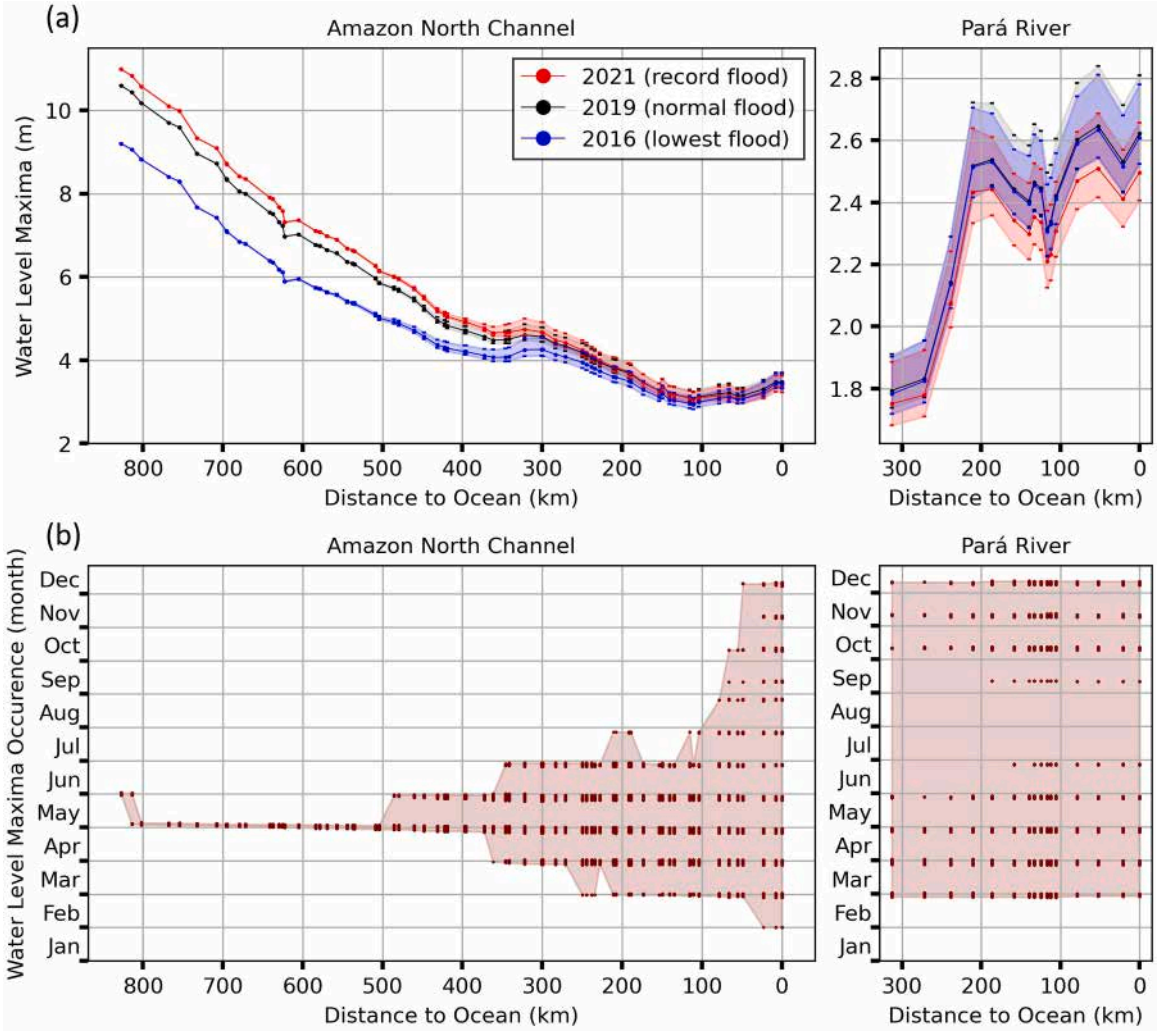

Fig. 8. (a) Mean value of yearly maxima distribution in Amazon North Channel and Pará River for 2016, 2019 and 2021. Min-max deviation is also displayed. Water level maxima is calculated with respect to Mean Sea Level. (b) Hovmoller diagram of the yearly water level maxima occurrence during 2021 in Amazon North Channel and Pará River.

4.1. Comprehensive description of the water level maxima along the estuary

The 2021 peak discharge observed in Óbidos is 10 % above the seasonal climatology computed over the past decade. We investigated the impact of the discharge excess of the 2021 flood on the total water level along the estuary. For this, we compared the yearly maxima simulated by our model (*REF* simulation) during three contrasting years in terms of Amazon discharge (Fig. 1): 2021 (year of the record-breaking flood), 2019 (a near-normal year for the past decade in terms of Amazon discharge, with a peak discharge hardly 3 % above climatology), and 2016 (a year of minor flood, the flood during one of the driest year of the past decade, 15 % below climatology).

Fig. 8a shows the mean value of yearly water level maxima along the estuary (solid lines) and the difference between the maximum and the minimum values reached during yearly maxima (seen as the shaded envelope of each curve), separately for 2016, 2019 and 2021. The mean value of yearly water level maxima is computed across all the 44 h of yearly maximum water levels at each model point available along the course of the river. We distinguished the main course of the Amazon (the North Channel, on the north-western edge of the delta) and the Pará River (which forms the eastern-most arm of the delta). The stretches along which we computed the mean values of yearly water level maxima are visible Fig. 5a.

In 2021, water level maxima range from 11 m in Óbidos at the upstream limit of the estuary, to 2.9 m in the downstream part close to the oceanic mouth. Throughout the upper 300 km of the estuary, the 2021 maxima lie 30 to 40 cm higher than those of 2019. Further downstream, around 380 km from the ocean, the 2021 and 2019 maxima values become similar, with their envelopes overlapping. They remain similar throughout the downstream half of the estuary, down to the ocean. If we compare 2021 with 2016, the excess for 2021 amounts to 1.78 m in Óbidos, and remains larger than 0.4 m until 370 km upstream of the ocean. Over the 150 km downstream-most reach of the estuary, the maxima of 2021 are not significantly higher than those of 2016. Therefore, in the Amazon North Channel, the 2021 flood has a sensible signature on the maximum water level (of order 10 % excess compared to the extreme reached during a normal year) that is restricted to the upper half of the estuary, upstream of 380 km.

We also investigated the period when the water level maxima occur during the 2021 year (Fig. 8b). It appears that the window of occurrence of the water level maxima is narrow, typically between late April and early June, centered on the period of the peak flood in May (Fig. 1) all along the upstream part of the estuary down to 380 km inland. Further downstream, the temporal window of occurrence of the maxima spreads gradually, more and more as one progresses downstream. From 380 km upstream of the ocean, where the water level maximum of 2021 is no longer significantly different from that of the normal year 2019, the period prone to the occurrence of water level maxima gradually increases from one month, to 90 days in the next 50 kms, extending well after the date of the peak discharge. Further downstream, around 200 km, this spread is even larger, with water level maxima occurring anytime between 1st March and 25th July. Further downstream, throughout the downstream-most 30 km, the water level maxima are seen to occur anytime between late January and mid-December, that is even several months before or after the flood season. This shows that the downstream-ward decrease in the magnitude of the anomalous water level reached in 2021 coincides with a lengthening of the period of occurrence of the water level maxima: from 380 km to further downstream, water level maxima are no longer phase-locked with the timing of the peak discharge. Altogether, this suggests that the peak discharge anomaly of 2021 has a prominent influence on the occurrence of water level maxima only over the upstream half of the estuary, and not over the downstream half.

For the Pará River (Fig. 8c), the picture is strikingly different from the Northern Channel of the Amazon. Indeed, 2021 no longer appears as a year of water level maxima higher than the maxima that occurred during the other years. The magnitudes of the yearly maxima of the various years widely overlap along the whole river stretch, ranging from 1.7 m to 2.8 m. 2016 and 2021 yearly maxima are roughly the same, with 2019 maxima slightly exceeding (by a handful of cm) that of 2016 on the oceanic side. The 2021 yearly maxima are globally lower than 2019 and 2016 distribution, by 10 cm typically.

To investigate more in depth the signature of the 2021 flood on the upstream dynamics of the Amazon North Channel, we focused on the two following features of the estuarine dynamics: first, the total water level at Santarém (location visible on Fig. 1), the largest city of the upper estuary; second, the water volume stored in the Monte Alegre floodplain, situated downstream of Santarém.

4.2. Upper estuary dynamics

4.2.1. Water level in Santarém

Santarém is located 780 km upstream of the oceanic mouths, 120 km downstream of Óbidos, the upper limit of the estuary. Fig. 9 shows the water level simulated at Santarém for 2019 and 2021, during the March-July flood season.

The 2021 water level maxima occurred in the beginning of May, almost one month before the peak discharge of the Amazon occurring on the 30th of May. This one-month advance is explained by the contribution of the Tapajós, which is the main tributary of the Amazon over our domain (Fig. 1c) and which timing of the seasonal flood is in advance with regards to that of the Amazon (not shown). This coincides with a peak of the intra-monthly oscillations seen throughout the period. These peaks are due to the presence of significant long-period tidal constituents (MSf and Mm) (Gabioux et al., 2005; Fassoni-Andrade et al., 2023a). Such an amplitude (around 12 cm, not shown) of Mm and MSf low-frequency tidal signal during high flow far upstream is in line with the estuarine dynamics described in Guo et al. (2020). Both 2019 and 2021 water levels stand above the seasonal climatology throughout the flood period.

Water level maxima reached 9.1 m in 2021, that is 40 cm higher than the maximum value of 8.7 m reached in 2019. The 2021 water level lies above the 2019 maximum water level for approximately 1 month.

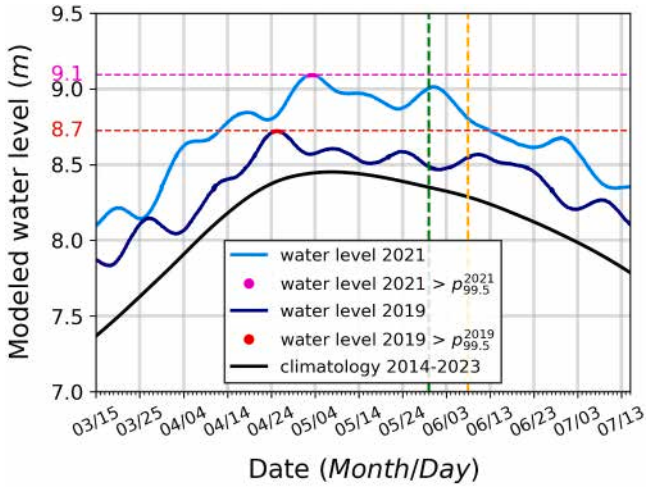

Fig. 9. Modeled water level in Santarém, in the upstream estuary, between 15th March and 15th July. Blue line (Dark blue line) represents total modeled water level in 2021 (in 2019) from *REF* simulation. The pink dots (red dots) mark the yearly water level maxima in 2021 (in 2019). The black line is the 2014–2023 water level climatology. The horizontal dotted lines represent the highest instance of the water level maxima, for each of the two years. The vertical green dotted line marks the peak discharge of 2021 occurring on the 30th of May at Óbidos. The orange dotted line marks the peak discharge of 2019 occurring on the 8th of June.

4.2.2. Water volume in Monte Alegre floodplain

We also assessed the year-to-year variability of the volume of water stored in the Monte Alegre floodplain (Fig. 10), situated 50 km downstream Santarém, comparing the situations among 2021 and 2019. As seen in Fig. 9, the water volume shows a low-frequency rise-and-fall evolution during the flood season, with maximum storage in May. Above this low-frequency evolution, intra-monthly oscillations are seen, with apparent timescales of about 2 to 4 weeks. This is consistent with the signature of 14 day-period and 28 day-period tidal waves propagating inside the floodplain from the Amazon mainstem, as the floodplain is connected to the Amazon River where such tidal frequencies are known to exist (Fassoni-Andrade et al., 2023a). Moreover, the water volume for both 2019 and 2021 remains superior to that of the seasonal climatology consistently throughout the flood season, suggesting the prominent imprint of the discharge anomaly thanks to the hydraulic connectivity between the floodplain and the Amazon mainstem. Water volume reached 6.25 km^3 during the 2021 flood, against 5.86 km^3 in 2019. This amounts to an increase of 7 % in the water volume stored in the floodplain. These findings echo to the recent study in the Curuai floodplain located 150 km upstream of Monte Alegre floodplain (Fassoni-Andrade et al., 2023b). Also, the model simulates a water storage in 2021 that remains above the maximum of 2019 consistently for 2.5 months (from 12th April to 12th June).

4.3. Dynamics of water level maxima along the estuary

To gain a comprehensive view of the imprint of the 2021 flood on the whole estuary, we quantified the role of the various forcing factors on the 2021 and 2019 water level maxima from upstream to downstream. Following the method exposed in Section 2.4, we isolated the part attributable to the discharge ($DISCH_{contribution}$), to the tide ($TIDE_{contribution}$) and to the atmosphere ($ATM_{contribution}$). Following our findings of Section 6.1, we investigated separately the main channel of the Amazon (North Channel) and the Pará channel. Fig. 11 displays the result of this analysis, expressed in terms of mean anomalies of the total water level during the yearly extremes with respect to its seasonal climatology.

Along the Amazon North Channel, the model suggests three successive regimes, from the upstream estuary to the downstream region. Over the upstream part (viz. the upper 450 km), the anomaly of water level during the occurrences of the yearly maxima is around 30 cm higher in 2021 than in 2019 (black and grey curves in Fig. 11a). This is mostly explained by the discharge contribution (red curve), that is twice higher in 2021 vs. 2019 (70 % vs 35 % for the most part). The tide contribution is nearly the same for both years, accounting for around 5 cm upstream to 40 cm downstream. As for the atmospheric contribution, it is higher in 2019, ranging from 2 cm to 10 cm, vs. 4 cm to 7 cm in 2021, translating into a much higher relative contribution in maxima generation for 2019 (around 20 %) compared to 2021 (around 7 %).

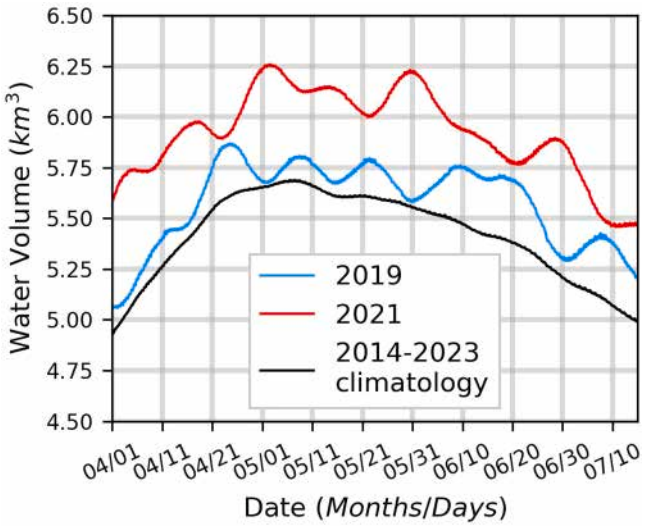

Fig. 10. Water volume contained in Monte Alegre floodplain calculated from the model during the flood period, between 1st of April and 15th of July. Red line (blue line) shows the water volume in 2021 (in 2019). The 2014–2023 climatology of the water volume is displayed in back line.

In the mid-estuary, between 350 km and 280 km, the anomaly is roughly the same between 2019 and 2021. There, the absolute contribution of the tide increases more vividly as the discharge contribution starts to diminish.

Further downstream, over the terminal part of the estuary, from 280 km to the open ocean, the anomaly from 2019 gradually surpasses 2021 from 2 cm to 14 cm, caused by the drastic reduction of the discharge contribution for both years, even becoming negative for both years around 200 km, along with an important increase in the tidal contribution. The 2019 tidal contribution is typically 10 cm to 20 cm larger than the 2021 contribution.

For the Pará River, the 2021 flood did not induce any remarkable extreme event of the water level (Section 4.1.). Fig. 11bd shows that this is partly explained by the lesser contribution of the discharge in 2021, compared to 2019 (typically by a few centimeters). We remind that the model is forced by the discharges of various rivers, but that only the Amazon comprises interannual variability (Fig. 3d). Tocantins River, outflowing at the upstream limit of the Pará, is prescribed in the model as a seasonal climatology, due to the lack of runoff data. Hence its contribution on the occurrence of water level maxima is not assessed here. In other words, our framework allows to quantify the influence of the Amazon flood on the Pará hydrodynamics, keeping in mind that the two branches of the delta are connected via the Breves Channel and via the ocean. Globally, the water level maxima in the Pará are prominently driven by the tide, with a relative contribution of >95 % all along its course, for both years. The atmospheric surges have a sensible contribution in the upstream part of the Pará (up to 7 %). In contrast, the Amazon flood does not contribute to the occurrence of water level maxima in the Pará.

5. Discussion and conclusion

The 30th of May 2021 peak flood was recorded as the highest in 12 years, and 2nd highest in 56 years, in Óbidos at the upstream limit of Amazon estuary. Thanks to a state-of-the-art cross-scale modeling of the whole estuarine continuum of the Amazon estuary, including the various branches of its terminal delta, the present study shows that this record-breaking flood had a contrasted spatial influence in the water level dynamics along the estuary. In the Amazon North Channel, the imprint of this anomaly in terms of extreme water level extends from Óbidos (800 km upstream of the oceanic mouths) to 380 km downstream. The magnitude of the water level maxima, around 60 cm higher than the seasonal climatology, is very significant. The underlying mechanism of water level maxima generation largely results from the effect of the anomalous Amazon discharge. Further downstream, the water level maxima of 2021 do not significantly differ from the regime of a normal year (2019). This can be explained by the growing influence of the tide in the overall variability of the water level, over the lower half of the estuary. Our model shows that the impact of the May 2021 flood on the occurrence of water level maxima is restricted to the Amazon mainstem and does not extend inside the Pará stretch that we analyzed (that forms the eastern arm of the Amazon delta).

Despite the particular attention given to the model calibration and validation, our modeling framework presents several limitations. First, the realism of the modeled tide in the downstream part of the estuary remains perfectible, on account of the relatively poorly known bathymetry of the coastal ocean there. Another potentially important source of error concerns the discharge condition observed in Óbidos,

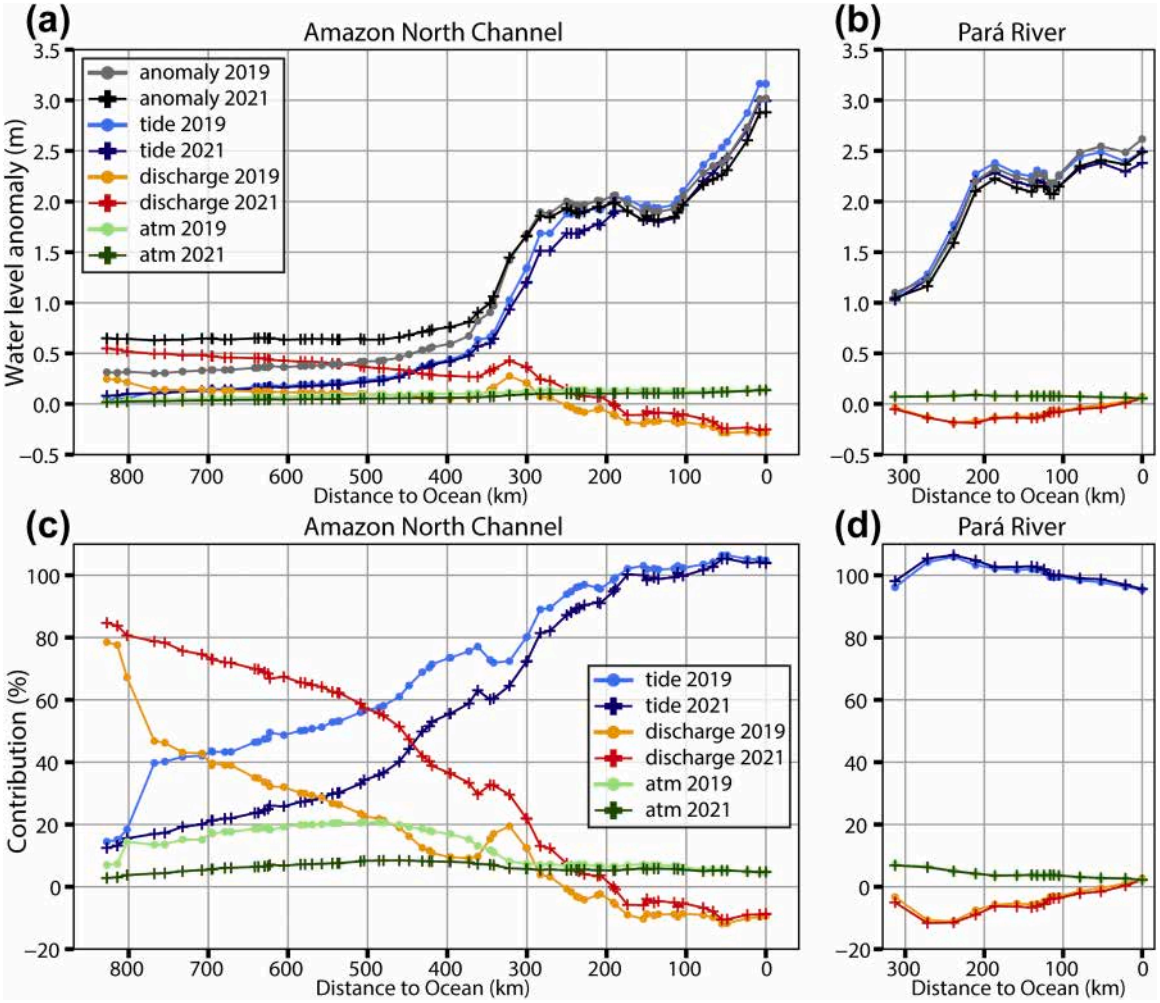

Fig. 11. Mean anomaly of total water level (Eq. (6)) during yearly maxima with respect to 2014–2023 climatology (black and grey lines) in Amazon North Channel (a) and Pará River (b). The mean contributions of the various forcing factors during yearly maxima for both years are shown in colors, namely the tide (light and dark blue), the discharge (red and orange) and the atmosphere (light and dark green). (c) and (d) same as (a) and (b) respectively but expressed in percent of the total anomaly.

prescribed in the model through its upstream open boundary. The level of accuracy of the available observations remains unknown. Being a huge freshwater flux, and even more so during the flood period that forms the focus of the present study, an uncertainty of even a few percents of the Amazon discharge is bound to have sensible impact on the hydrodynamics modeled along the estuarine continuum. These limitations call for a re-visit of the present findings once updated datasets become available to ease the hydrodynamic modeling.

Nevertheless, at a time when the hydrological cycle over the Amazon watershed is getting intensified and keeping in mind the potentially profound impacts of the water level extremes over the ecology and over the growing population of the banks of the Amazon estuary (Junk et al., 2014; Mansur et al., 2016), our study paves the way for an assessment of the multi-faceted risks associated with the recurring floods of this mega-hydrosystem.

CRediT authorship contribution statement

Paul Coulet: Writing – original draft, Software, Methodology, Investigation, Formal analysis, Conceptualization. **Fabien Durand:** Writing – review & editing, Methodology, Investigation, Data curation, Conceptualization. **Alice Fassoni-Andrade:** Methodology. **Jamal Khan:** Writing – review & editing, Formal analysis. **Laurent Testut:** Writing – review & editing, Conceptualization. **Florence Toublanc:** Writing – review & editing, Methodology. **Leandro Guedes Santos:** Investigation, Data curation. **Daniel Medeiros Moreira:** Investigation, Funding acquisition, Data curation.

Declaration of competing interest

The authors declare that they have no known competing financial interests or personal relationships that could have appeared to influence the work reported in this paper.

Acknowledgements

Open access funding provided by Université de Toulouse. This research has been supported by Horizon 2020 (EOSC-SYNERGY project, grant number 857647), IRD and CNES (through a TOSCA funding). We are thankful to Marinha do Brasil, IBGE, ANA, CPRM and SO HYBAM-IRD for the provision of the tide gauge records. Supercomputing facilities were provided by the HPC resources of IDRIS (France) under the project# GEN7298 granted by GENCI. This study has been supported through the grant EUR TESS N°ANR-18-EURE-0018 in the framework of the Programme des Investissements d'Avenir.

Data availability

Data will be made available on request.

References

Allain, D.J., 2016. TUGOm Tidal Toolbox. ftp://ftp.legos.obs-mip.fr/pub/ecola/tools/ttb.pdf.

Andersen, O.B., Woodworth, P.L., Flather, R.A., 1995. Intercomparison of recent ocean tide models. J. Geophys. Res. Ocean. 100, 25261–25282. https://doi.org/10.1029/95JC02642.

Beardsley, R.C., Candela, J., Limeburner, R., Geyer, W.R., Lentz, S.J., Castro, B.M., Cacchione, D., Carneiro, N., 1995. The M2 tide on the Amazon Shelf. J. Geophys. Res. 100 (C2), 2283–2319. https://doi.org/10.1029/94JC01688.

Beveridge, C.F., Espinoza, J.-C., Athayde, S., Correa, S.B., Couto, T.B.A., Heilpern, S.A., Jenkins, C.N., Piland, N.C., Utsunomiya, R., Wongchuig, S., Anderson, E.P., 2024. The Andes–Amazon–Atlantic pathway: a foundational hydroclimate system for social–ecological system sustainability. Proc. Natl. Acad. Sci. U.S.A. 121, e2306229121. https://doi.org/10.1073/pnas.2306229121.

Birol, F., Fuller, N., Lyard, F., Cancet, M., Niño, F., Delebecque, C., Fleury, S., Toublanc, F., Melet, A., Saraceno, M., Léger, F., 2017. Coastal applications from nadir altimetry: example of the X-TRACK regional products. Adv. Space Res. 59, 936–953. https://doi.org/10.1016/j.asr.2016.11.005.

Callède, J., Cochonneau, G., Alves, F.V., Guyot, J.-L., Guimarães, V.S., De Oliveira, E., 2010. Les apports en eau de l'Amazone à l'Océan Atlantique. J. Water Sci. 23, 247–273. https://doi.org/10.7202/044688ar.

Callède, J., Moreira, D.M., Calmant, S., 2013. Détermination de l'altitude du Zéro des stations hydrométriques en amazonie brésilienne. Application aux lignes d'eau des Rios Negro, Solimões et Amazone. J. Water Sci. 26, 153–171. https://doi.org/10.7202/1016065ar.

Chevuturi, A., Klingaman, N.P., Woolnough, S.J., Rudorff, C.M., Coelho, C.A.S., Schöngart, J., 2023. Forecasting annual maximum water level for the Negro River at Manaus using dynamical seasonal predictions. Clim. Serv. 30, 100342. https://doi.org/10.1016/j.cliser.2023.100342.

Codiga, D.L., 2011. Unified tidal analysis and prediction using the UTide Matlab functions. https://doi.org/10.13140/RG.2.1.3761.2008.

Coulet, P., Durand, F., Fassoni-Andrade, A., Khan, M.J.U., Testut, L., Toublanc, F., Santos, L.G., Moreira, D.M., Azevedo, A., 2025. Dynamics of yearly maximum water levels in the Amazon Estuary. Estuaries Coasts 48, 54. https://doi.org/10.1007/s12237-025-01483-7.

Durand, F., Testut, L., Jouanno, J., Fassoni-Andrade, A.C., 2022. Role of the amazon outflow on the barotropic tide on the amazonian shelf. Cont. Shelf Res. 238, 104695. https://doi.org/10.1016/j.csr.2022.104695.

Dronkers, J.J., 1964. Tidal computations in rivers and coastal waters. NL: North Holland Publishing Company, 518 pp.

Eslami, S., Hoekstra, P., Kernkamp, H., Nguyen Trung, N., Do Duc, D., Tran Quang, T., Februarianto, M., Van Dam, A., Van Der Vegt, M., 2019. Flow division dynamics in the Mekong Delta: application of a 1D-2D coupled model. Water (Basel) 11, 837. https://doi.org/10.3390/w11040837.

Espinoza, J.-C., Marengo, J.A., Schongart, J., Jimenez, J.C., 2022. The new historical flood of 2021 in the Amazon River compared to major floods of the 21st century: atmospheric features in the context of the intensification of floods. Weather and climate extremes 35, 100406. https://doi.org/10.1016/j.wace.2021.100406.

Fang, G., Wang, Y., Wei, Z., Choi, B.H., Wang, X., Wang, J., 2004. Empirical cotidal charts of the Bohai, Yellow, and East China Seas from 10 years of TOPEX/Poseidon altimetry. J. Geophys. Res. 109, 2004JC002484. https://doi.org/10.1029/2004JC002484.

Fassoni-Andrade, A.C., Paiva, R.C.D.D., Rudorff, C.D.M., Barbosa, C.C.F., Novo, E.M.L.D.M., 2020. High-resolution mapping of floodplain topography from space: a case study in the Amazon. Remote Sens. Environ. 251, 112065. https://doi.org/10.1016/j.rse.2020.112065.

Fassoni-Andrade, A.C., Durand, F., Moreira, D., Azevedo, A., Dos Santos, V.F., Funi, C., Laraque, A., 2021. Comprehensive bathymetry and intertidal topography of the Amazon estuary. Earth Syst. Sci. Data 13, 2275–2291. https://doi.org/10.5194/essd-13-2275-2021.

Fassoni-Andrade, A.C., Durand, F., Azevedo, A., Bertin, X., Santos, L.G., Khan, J.U., Testut, L., Moreira, D.M., 2023a. Seasonal to interannual variability of the tide in the Amazon estuary. Cont. Shelf. Res. 255, 104945. https://doi.org/10.1016/j.csr.2023.104945.

Fassoni-Andrade, A., Cauduro Dias De Paiva, R., Wongchuig, S., Barbosa, C., Durand, F., Sanna Freire Silva, T., 2023b. Expressive fluxes over Amazon floodplain revealed by 2D hydrodynamic modelling. J. Hydrol. 625, 130122. https://doi.org/10.1016/j.jhydrol.2023.130122.

Flather, R.A., 1976. A tidal model of the north-west European continental shelf. Mémoires de La Société Roy. des Sci. de Liège 6 (10), 141–164.

Gabioux, M., Vinzon, S.B., Paiva, A.M., 2005. Tidal propagation over fluid mud layers on the Amazon shelf. Cont. Shelf. Res. 25, 113–125. https://doi.org/10.1016/j.csr.2004.09.001.

Gallo, M.N., Vinzon, S.B., 2005. Generation of overtides and compound tides in Amazon estuary. Ocean Dyn. 55, 441–448. https://doi.org/10.1007/s10236-005-0003-8.

Godin, G., 1985. Modification of river tide by the discharge. J. Waterw. Port Coastal Ocean Eng. 111 (2), 257–274. https://doi.org/10.1061/(ASCE)0733-950X(1985)111:2(257).

Godin, G., 1999. The propagation of tides up rivers with special considerations on the Upper Saint Lawrence River. Estuar. Coast. Shelf. Sci. 48, 307–324. https://doi.org/10.1006/ecss.1998.0422.

Guo, L., Zhu, C., Wu, X., Wan, Y., Jay, D.A., Townend, I., Wang, Z.B., He, Q., 2020. Strong inland propagation of low-frequency long waves in river estuaries. Geophys. Res. Lett. 47, e2020GL089112. https://doi.org/10.1029/2020GL089112.

Haigh, I., Nicholls, R., Wells, N., 2010. Assessing changes in extreme sea levels: application to the English Channel, 1900–2006. Cont. Shelf. Res. 30, 1042–1055. https://doi.org/10.1016/j.csr.2010.02.002.

Huang, W., Ye, F., Zhang, Y.J., Park, K., Du, J., Moghimi, S., Myers, E., Pe'eri, S., Calzada, J.R., Yu, H.C., Nunez, K., Liu, Z., 2021. Compounding factors for extreme flooding around Galveston bay during Hurricane Harvey. Ocean Model. (Oxf) 158, 101735. https://doi.org/10.1016/j.ocemod.2020.101735.

Junk, W.J., Piedade, M.T.F., Lourival, R., Wittmann, F., Kandus, P., Lacerda, L.D., Bozelli, R.L., Esteves, F.A., Nunes Da Cunha, C., Maltchik, L., Schöngart, J., Schaeffer-Novelli, Y., Agostinho, A.A., 2014. Brazilian wetlands: their definition, delineation, and classification for research, sustainable management, and protection. Aquatic Conserv. 24, 5–22. https://doi.org/10.1002/aqc.2386.

Khan, M.J.U., Durand, F., Testut, L., Krien, Y., Islam, A.K.M.S., 2020. Sea level rise inducing tidal modulation along the coasts of Bengal delta. Cont. Shelf. Res. 211, 104289. https://doi.org/10.1016/j.csr.2020.104289.

Kineke, G.C., Sternberg, R.W., 1992. Measurements of high concentration suspended sediments using the optical backscatterance sensor. Mar. Geol. 108, 253–258. https://doi.org/10.1016/0025-3227(92)90199-R.

Kineke, G.C., Sternberg, R.W., 1995. Distribution of fluid muds on the Amazon continental shelf. Mar. Geol. 125, 193–233. https://doi.org/10.1016/0025-3227(95)00013-O.

Kosuth, P., Callède, J., Laraque, A., Filizola, N., Guyot, J.L., Seyler, P., Fritsch, J.M., Guimarães, V., 2009. Sea-tide effects on flows in the lower reaches of the Amazon River. Hydrol. Process 23, 3141–3150. https://doi.org/10.1002/hyp.7387.

Krien, Y., Mayet, C., Testut, L., Durand, F., Tazkia, A.R., Islam, A.K.M.S., Gopalakrishna, V.V., Becker, M., Calmant, S., Shum, C.K., Khan, Z.H., Papa, F., Ballu, V., 2016. Improved bathymetric dataset and tidal model for the Northern Bay of Bengal. Marine Geodesy 39, 422–438. https://doi.org/10.1080/01490419.2016.1227405.

Le Bars, Y., Lyard, F., Jeandel, C., Dardengo, L., 2010. The AMANDES tidal model for the Amazon estuary and shelf. Ocean Model (Oxf) 31, 132–149. https://doi.org/10.1016/j.ocemod.2009.11.001.

Lyddon, C., Brown, J.M., Leonardi, N., Plater, A.J., 2018. Uncertainty in estuarine extreme water level predictions due to surge-tide interaction. PLoS One 13, e0206200. https://doi.org/10.1371/journal.pone.0206200.

Mansur, A.V., Brondízio, E.S., Roy, S., Hetrick, S., Vogt, N.D., Newton, A., 2016. An assessment of urban vulnerability in the Amazon Delta and Estuary: a multi-criterion index of flood exposure, socio-economic conditions and infrastructure. Sustain Sci. 11, 625–643. https://doi.org/10.1007/s11625-016-0355-7.

Marengo, J.A., Espinoza, J.C., 2016. Extreme seasonal droughts and floods in Amazonia: causes, trends and impacts. Int. J. Climatol. 36, 1033–1050. https://doi.org/10.1002/joc.4420.

Matte, P., Secretan, Y., Morin, J., 2017. Hydrodynamic modeling of the St. Lawrence Fluvial Estuary. II: reproduction of spatial and temporal patterns. J. Waterway, Port, Coastal, Ocean Eng. 143, 04017011. https://doi.org/10.1061/(ASCE)WW.1943-5460.0000394.

Nittrouer, C.A., Kuehl, S.A., Figueiredo, A.G., Allison, M.A., Sommerfield, C.K., Rine, J.M., Faria, L.E.C., Silveira, O.M., 1996. The geological record preserved by amazon shelf sedimentation. Cont. Shelf Res. 16, 817–841. https://doi.org/10.1016/0278-4343(95)00053-4.

Pekel, J.-F., Cottam, A., Gorelick, N., Belward, A.S., 2016. High-resolution mapping of global surface water and its long-term changes. Nature 540, 418–422. https://doi.org/10.1038/nature20584.

Potapov, P., Li, X., Hernandez-Serna, A., Tyukavina, A., Hansen, M.C., Kommareddy, A., Pickens, A., Turubanova, S., Tang, H., Silva, C.E., Armston, J., Dubayah, R., Blair, J.B., Hofton, M., 2021. Mapping global forest canopy height through integration of GEDI and Landsat data. Remote Sens. Environ. 253, 112165. https://doi.org/10.1016/j.rse.2020.112165.

Pugh, D., Woodworth, P., 2014. Sea-Level Science: Understanding Tides, Surges, Tsunamis and Mean Sea-Level Changes. Cambridge University Press, Cambridge. https://doi.org/10.1017/CBO9781139235778.

Rosário, R.P., Borba, T.A.C., Santos, A.S., Rollnic, M., 2016. Variability of salinity in Pará river estuary: 2D analysis with flexible mesh model. J. Coast. Res. 75, 128–132. https://doi.org/10.2112/SI75-026.1.

Ruault, V., Jouanno, J., Durand, F., Chanut, J., Benshila, R., 2020. Role of the tide on the structure of the Amazon plume: a numerical modeling approach. JGR Oceans 125, e2019JC015495. https://doi.org/10.1029/2019JC015495.

Saha, S., Moorthi, S., Wu, X., Wang, J., Nadiga, S., Tripp, P., Behringer, D., Hou, Y.-T., Chuang, H., Iredell, M., Ek, M., Meng, J., Yang, R., Mendez, M.P., Dool, H.van den, Zhang, Q., Wang, W., Chen, M., Becker, E., 2011. NCEP climate forecast system version 2 (CFSv2) selected hourly time-series products. https://doi.org/10.5065/D6N877VB.

Testut, L., Unnikrishnan, A.S., 2016. Improving modeling of tides on the continental shelf off the west coast of India. Coas 32, 105–115. https://doi.org/10.2112/JCOASTRES-D-14-00019.1.

Zhang, K., Douglas, B.C., Leatherman, S.P., 2000. Twentieth-century storm activity along the U.S. East Coast. J. Climate 13, 1748–1761. https://doi.org/10.1175/1520-0442(2000)013≤1748:TCSAAT≥2.0.CO;2.

Zhang, Y.J., Ye, F., Stanev, E.V., Grashorn, S., 2016. Seamless cross-scale modeling with SCHISM. Ocean Model. (Oxf) 102, 64–81. https://doi.org/10.1016/j.ocemod.2016.05.002.

Zhang, Y.J., Anderson, J., Park, K., Wu, C.H., Wipperfurth, S., Anderson, E., Pe'eri, S., Beletsky, D., Titze, D., Di Lorenzo, E., Moghimi, S., Seroka, G., Myers, E., Fujisaki-Manome, A., Kelley, J., 2024. Debunking common myths in coastal circulation modeling. Ocean Model. (Oxf) 190, 102401. https://doi.org/10.1016/j.ocemod.2024.102401.